THE JOURNAL OF PHYSICAL CHEMISTRY Letters

Letter

pubs.acs.org/JPCL

When and Why Like-Sized, Oppositely Charged Particles Assemble into Diamond-like Crystals

Kyle J. M. Bishop,*[,†] Nicolas R. Chevalier,[‡] and Bartosz A. Grzybowski*[,‡]

[†]Department of Chemical Engineering, The Pennsylvania State University, 132C Fenske Lab, University Park, Pennsylvania 16802, United States

[‡]Department of Chemical and Biological Engineering and Department of Chemistry, Northwestern University, 2145 Sheridan Road, Evanston, Illinois 60208, United States

Supporting Information

ABSTRACT: Like-sized, oppositely charged nanoparticles are known to assemble into large crystals with diamond-like (ZnS) ordering, in sharp contrast to analogous molecular ions and micrometer-scale colloids, which invariably favor more closely packed structures (NaCl or CsCl). Here, we show that these experimental observations can be understood as a consequence of ionic screening and the slight asymmetry in surface charge present on the assembling particles. With this asymmetry taken into account, free-energy calculations predict that the diamond-like ZnS lattice is more favorable than other 1:1 ionic structures, namely, NaCl or CsCl, when the Debye screening length is considerably larger than the particle size. A thermodynamic model describes how the presence of neutralizing counterions within the interstitial regions of the crystal acts to bias the formation of low-volume-fraction structures. The results provide general insights into the self-assembly of non-close-packed structures via electrostatic interactions.

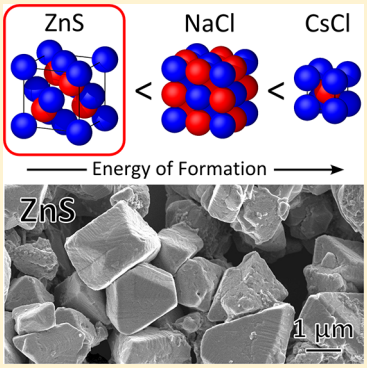

SECTION: Glasses, Colloids, Polymers, and Soft Matter

Colloidal crystals characterized by diamond-like (ZnS) internal ordering have long been studied[1−3] due to the fundamental interest in this non-closed-packed structure (packing fraction of only 0.34) and potential applications as photonic materials exhibiting a complete band gap in all directions.[4−7] At the microscale, such "artificial diamonds" have been constructed by robotic manipulation,[8] self-assembled from more complex tetrahedral precursors,[9] or grown over small areas of surface-templated colloids.[10,11] At the same time, potentially more efficient schemes based on self-assembly of microparticles from solution have so far proven unsuccessful and have invariably led to close-packed crystals with higher packing fractions.[12−14] On the other hand, we have shown[15,16] that these limitations can be overcome at the nanoscale, where equally sized, oppositely charged nanoparticles self-assemble into large, diamond-like crystals, each composed of tens of thousands to tens of millions of nanoparticles (Figure 1a). In the original experimental study,[15] we proposed that the formation of these structures is the result of screening effects due to the counterions surrounding each NP.

Here, we take this analysis further and argue that while screening is an important factor, the formation of artificial diamonds by electrostatic forces also requires a slight asymmetry, in fact, seen in the original experiment, between the surface charge on positive and negative NPs. With this asymmetry taken into account, free-energy calculations predict that the diamond-like ZnS lattice is more favorable than alternative 1:1 ionic structures (namely, NaCl or CsCl) when the Debye screening length is considerably larger than the particle size. These results are interpreted by a thermodynamic model that describes how the presence of neutralizing counterions within the interstitial regions between the NPs can bias the formation of low-volume-fraction structures. The virtue of our approach is that it rationalizes previous experiments and delineates the phase space over which diamond-like crystals can form without postulating complex and/or physically unrealistic interparticle potentials previously proposed to guide formation of diamond-like colloidal crystals.[17,18]

The experimental system[15] modeled here is comprised of Au and Ag nanoparticles with mean diameters of 5.1 and 4.8 nm, respectively, and coated with oppositely charged, ω-functionalized alkane thiols,[19] $HS(CH_2)_{10}COO^-$ [MUA] and $HS(CH_2)_{11}NMe_3^+$ [TMA] (Figure 1a). The thicknesses of the self-assembled monolayers (SAMs) coating the NPs are ∼1.6 nm for MUA and ∼1.9 nm for TMA; consequently, negatively charged AuMUA NPs are very similar in size to positively charged AgTMA NPs (total particle diameter, $D \approx 8.5$ nm). Importantly, owing to slight differences in the diameters of the NP cores, AuMUA NPs are covered by slightly more ligands than AgTMA NPs. Assuming equal thiol binding areas for Au and Ag surfaces (∼0.21 nm^2),[20,21] the ratio of positive ligands

Received: March 19, 2013
Accepted: April 10, 2013
Published: April 10, 2013

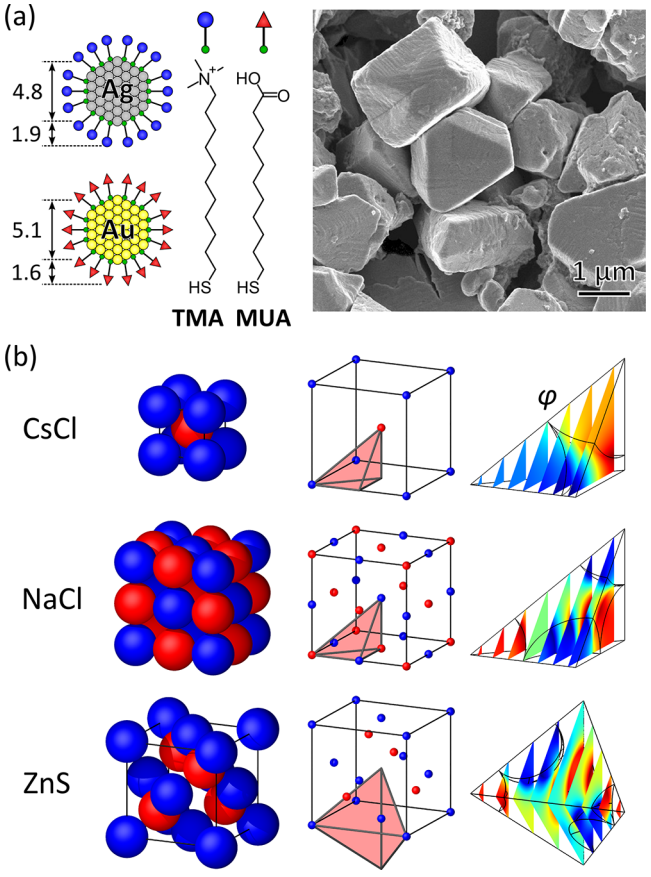

Figure 1. (a) The 1:1 mixtures of positively charged AgTMA NPs and negatively charged AuMUA NPs organize in solution to form micrometer-sized NP crystals with diamond-like, ZnS structure. (b) (Left) Three ionic lattices investigated, CsCl, NaCl, and ZnS. (Middle) Unit cells for the three lattices with the simulation cells highlighted in red. (Right) Electrostatic potential within the simulation cells for equal and oppositely charged particles with $\kappa a = 1$ and $\varepsilon_p/\varepsilon = 1$.

on a single AuMUA NP to negative ligands on a single AgTMA NP is ~1.1. This small asymmetry gives rise to an excess charge for each pair of oppositely charged NPs equal to $\Delta\sigma = \sigma_+ + \sigma_- \approx -0.1\sigma_+$, where $\sigma_\pm$ is the surface charge density on the respective particles. As we will show, the presence of counterions within the unit cell needed to neutralize the excess charge on the particles can act to shift the electrostatic free energy in favor of the diamond-like ZnS structure.

Micron-sized crystals are grown from 1:1 mixtures of positively and negatively charged NPs dispersed in 1:4 v/v mixtures of water and DMSO at 65 °C with the pH adjusted to >10 to fully deprotonate the MUA ligands.[15] Powder X-ray diffraction reveals that NPs are distributed on a diamond lattice (ZnS structure), as further supported by elemental composition measurements of the bulk crystals as well as STEM/EDS line scans of the crystals faces (for all experimental details, see ref 15). In the context of the present study, it is important to note that while the polydispersity of the NPs affects the quality of the NP supracrystals, it does not alter the diamond-like packing as each separate crystal that forms is composed of NPs of equal sizes (to within less than ~0.2 nm).[15] Consequently, we treat the NPs as monodisperse. Also, the magnitudes of the experimentally determined zeta potentials for NPs of either polarity do not exceed ±60 mV,[15] permitting the use of the linearized Poisson–Boltzmann equation to model the system's electrostatics.[22] Finally, as the oppositely charged NPs were washed repeatedly prior to crystallization to remove excess ions, the ion concentration during crystallization was at most ~0.1 mM (equal that of the charged ligands). This salt concentration corresponds to a screening length of $\kappa^{-1} \approx 40$ nm and a dimensionless screening parameter of $\kappa a \approx 0.1$, where $a \approx 4$ nm is the NP radius. Together, the screening parameter $\kappa a \approx 0.1$ and the excess charge $\Delta\sigma/\sigma_+ \approx -0.1$ serve to determine the energetically favored crystal structure, as shown below.

To first approximation, the problem of predicting the structure of a crystal assembling from a solution of oppositely charged NPs can be approached by comparing the (zero-temperature) energies of possible binary lattices. Because of the 1:1 stoichiometry of our NP mixture and of the assembling crystals, we limit our analysis to the relevant binary lattices, CsCl, NaCl, and ZnS (as opposed to, for instance, CaF_2; Figure 1b). In the model, particles are treated as monodisperse spheres with radius a and constant surface charge density $\sigma_\pm$. For simplicity, we approximate the core–shell structure of the NPs by a single homogeneous medium with an effective dielectric constant $\varepsilon_p \approx 38$, chosen such that the dielectric particle has the same polarizability as the core–shell (metal/SAM) particles used in experiments (see Supporting Information section 1). We emphasize that the choice of ε_p does not influence the conclusions of our analysis (see Supporting Information section 2). To calculate the electrostatic energy of the respective structures, we first solve for the electrostatic potential φ in and around the particles, accounting for screening due to mobile counterions within the interstitial regions between the particles.

Electric Potential. The electric potential φ within the interstitial space between the particles is governed by the linear Poissson–Boltzmann (PB) equation

$$\nabla^2\varphi = \kappa^2\varphi \qquad \text{in solution} \tag{1}$$

where $\kappa^{-1} = (\varepsilon\varepsilon_o k_B T/2e^2 n_o)^{1/2}$ is the screening length, ε is the dielectric constant of the solvent, ε_o is the vacuum permittivity, $k_B T$ is the thermal energy, e is the elementary charge, and n_o is the concentration of the monovalent electrolyte in the surrounding solution. The ions within the colloidal crystal are in equilibrium with those in the surrounding electrolyte, that is, the chemical potentials of ions inside and outside of the crystal are equal. Consequently, the screening length is determined by the salt concentration not inside of the crystal but rather in the bulk solution where the electric potential is zero. Inside of the particles, the electric potential is governed by Laplace's equation.

$$\nabla^2\varphi_\pm = 0 \text{ inside } +/- \text{ particles} \tag{2}$$

Rather than compute the potential throughout the unit cell with periodic boundary conditions, we divide the respective structures along planes of mirror symmetry to create smaller simulation cells (Figure 1b). By symmetry, the electric potential at the surface of the simulation cell must satisfy the condition

$$\mathbf{n}\cdot\nabla\varphi = 0 \qquad \text{or} \qquad \mathbf{n}\cdot\nabla\varphi_\pm = 0 \tag{3}$$

where $\mathbf{n}$ is the unit vector normal to the surface. In this way, the electric potential may be calculated using only a fraction of the entire unit cell (1/48th in the case of NaCl or CsCl, 1/12th in the case of ZnS). Furthermore, at the surface of each particle, Gauss's law relates the surface charge density σ to the electric potential as

dx.doi.org/10.1021/jz4006114 | J. Phys. Chem. Lett. 2013, 4, 1507–1511

$$\varepsilon_o(\varepsilon_p \nabla\varphi_\pm - \varepsilon\nabla\varphi)\cdot\mathbf{n} = \sigma_\pm \tag{4}$$

Together, eqs 1−4 fully specify the electric potential throughout the colloidal crystal. These equations are solved numerically within the simulation cell using a commercial finite element solver (COMSOL). Figure 1b shows the electric potential for equal and oppositely charged particles for the three different ionic structures.

Electrostatic Free Energy. For the linear PB equation with constant charge boundary conditions, the electrostatic free energy per unit area of surface is given by[23]

$$f_\pm = \frac{1}{2}\varphi_s\sigma_\pm \tag{5}$$

where φ_s denotes local potential on the particle surface and f is measured relative to an uncharged reference state. The total free energy of the simulation cell F_s is determined by integrating this expression over the surfaces of positive (S_+) and negative (S_-) particles.

$$F_s = \frac{1}{2}\sigma_+\int_{S_+}\varphi_s\,dS + \frac{1}{2}\sigma_-\int_{S_-}\varphi_s\,dS \tag{6}$$

To facilitate comparison between the three lattices, we normalize F_s by the number of ion pairs within the simulation cell, $F \equiv F_s/N_s$, with N_s = 1/48, 1/12, and 1/3, for CsCl, NaCl, and ZnS, respectively. Furthermore, we define the energy of crystallization ΔF as the change in energy accompanying the organization of the particles from solution

$$\Delta F = F - F_+^\infty - F_-^\infty \tag{7}$$

where $F_\pm^\infty$ is the free energy of +/− particles at infinite separation. The latter may be calculated explicitly as $F_\pm^\infty = 2\pi a^2\varphi_\pm^\infty\sigma_\pm$, where $\varphi_\pm^\infty$ is the surface potential at infinite separation, $\varphi_\pm^\infty = a\sigma_\pm/\varepsilon\varepsilon_o(1+\kappa a)$, obtained by solving eq 1 with the boundary condition from eq 4. Crystallization is energetically favorable when $\Delta F < 0$ and unfavorable when $\Delta F > 0$.

The electrostatic model outlined above is characterized by three dimensionless parameters characterizing three physical effects: (1) the extent of ion screening, κa, (2) the degree of charge asymmetry, σ_-/σ_+, and (3) the dielectric contrast between particles and the solvent, $\varepsilon_p/\varepsilon$. Below, we address each of these effects in turn and highlight their implications to the formation of ZnS structures.

Symmetric Particles. We first consider the case of particles with equal and opposite surface charge ($\sigma_-/\sigma_+ = -1$) and with dielectric constants equal to that of the solvent ($\varepsilon_p/\varepsilon = 1$, similar to the experimental value, $\varepsilon_p/\varepsilon \approx 0.7$; see Supporting Information section 2 for results when $\varepsilon_p/\varepsilon \neq 1$). Figure 2 shows the energy of crystallization ΔF (scaled by $F^* \equiv a^3\sigma_+^2/\varepsilon\varepsilon_o$) as a function of the screening parameter κa for the three ionic lattices. There are two limiting regimes: (1) a weak screening regime where the screening length is much larger than the particle size ($\kappa a \ll 1$) and (2) a strong screening regime where the screening length is much smaller than the particle size ($\kappa a \gg 1$).

In the limit of weak screening ($\kappa a \ll 1$), the energy approaches that of the analogous ionic lattices as characterized by Madelung constants, M, with M = 1.7627, 1.7476, and 1.6381 for CsCl, NaCl, and ZnS, respectively.[24] Specifically

$$\Delta F = -\frac{Mq^2}{4\pi\varepsilon\varepsilon_o d} = -2\pi MF^* \qquad \text{for } \kappa a \to 0 \tag{8}$$

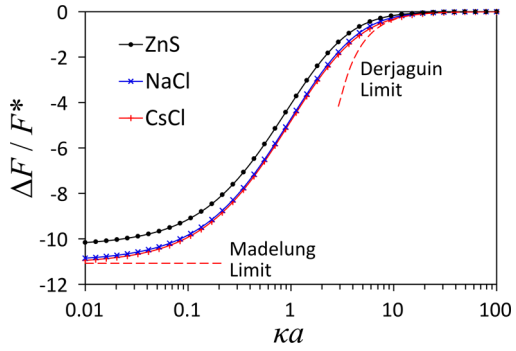

Figure 2. Symmetric particles. Electrostatic energy of crystallization (scaled by $F^* = a^3\sigma_+^2/\varepsilon\varepsilon_o$) as a function of the screening parameter κa for the three 1:1 ionic lattices (CsCl, NaCl, and ZnS). The open markers show the numerical results; the dashed curves show the limiting behaviors for weak screening ($\kappa a \gg 1$) and strong screening ($\kappa a \gg 1$) for the CsCl structure.

where q is the charge on each particle (here, $q = 4\pi a^2\sigma_+$) and d is the nearest-neighbor separation (here, $d = 2a$). This limit is illustrated for CsCl by the dashed curve in Figure 2. For equal and oppositely charged particles in the limit of large screening lengths, crystallization is energetically favorable in the order $\Delta F_{CsCl} < \Delta F_{NaCl} < \Delta F_{ZnS}$, meaning that formation of ZnS is the least favorable option.

In the limit of strong screening ($\kappa a \gg 1$), electrostatic interactions act over short length scales of order κ^{-1}; consequently, the electrostatic energy is well approximated by a pairwise sum over interactions between nearest neighbors. Using the Derjaguin approximation for constant charge surfaces[23,25]

$$\Delta F = -\frac{z\pi\ln(4)}{(\kappa a)^2}F^* \qquad \text{for } \kappa a \to \infty \tag{9}$$

where z is the number of nearest neighbors (z = 8, 6, and 4 for CsCl, NaCl, and ZnS). This limit is illustrated for CsCl by the dashed curve in Figure 2. Crystallization is favorable; however, the magnitude of the interaction is increasingly diminished by ion screening as κa is increased. Lattices with more nearest neighbors are energetically preferred, $\Delta F_{CsCl} < \Delta F_{NaCl} < \Delta F_{ZnS}$.

Thus, for symmetric particles ($\sigma_-/\sigma_+ = -1$ and $\varepsilon_p/\varepsilon = 1$), CsCl and NaCl structures are always energetically preferred over ZnS structures regardless of the extent of ion screening. This is not the case for asymmetric particles with different amounts of positive and negative charge.

Asymmetric Particles. When the net charge of the particles differs from zero ($\sigma_-/\sigma_+ \neq -1$), the excess charge, $\Delta\sigma = \sigma_+ + \sigma_-$, must be balanced by counterions within the unit cell to maintain overall charge neutrality. Interestingly, for *any* amount of excess charge $\Delta\sigma$, CsCl and NaCl are no longer favored over ZnS for all values of the screening parameter κa. Figure 3a presents the phase diagram showing the minimum-energy structure as a function of the excess charge $\Delta\sigma$ and the screening parameter κa. The diamond-like ZnS structure is favored over CsCl and NaCl structures when the screening parameter κa is of the same order of magnitude as the excess charge (scaled by σ_+), that is, when $\kappa a \approx |\Delta\sigma/\sigma_+|$. Interestingly, this corresponds closely to the experimental conditions described above, $\kappa a \approx 0.1$ and $|\Delta\sigma/\sigma_+| \approx 0.1$.

To understand these numerical results, it is helpful to re-examine the limits of large and small screening lengths in the case of "non-neutral" (in terms of NP charges) crystals. For

dx.doi.org/10.1021/jz4006114 | J. Phys. Chem. Lett. 2013, 4, 1507−1511

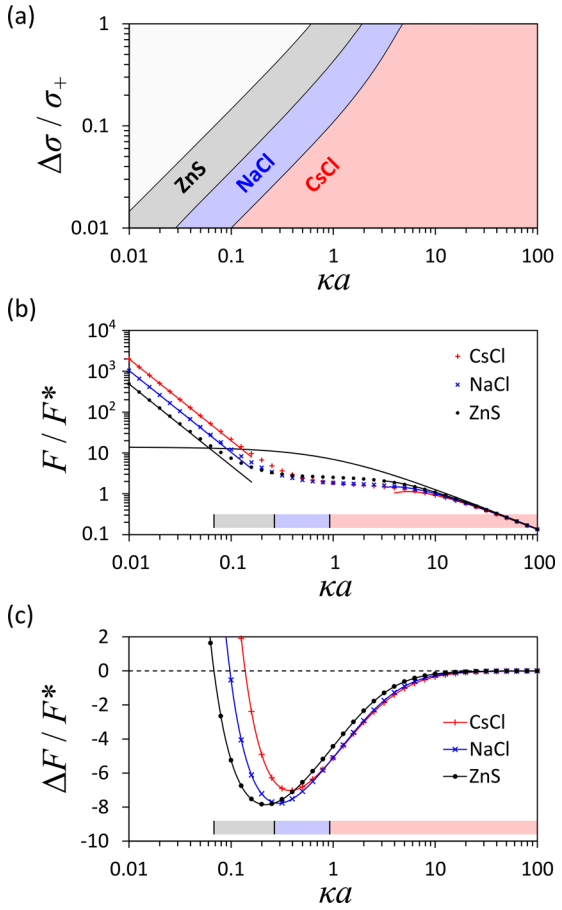

Figure 3. Charge asymmetric particles. (a) Phase diagram illustrating the energetically favored structure as a function of the excess charge $\Delta\sigma/\sigma_+$ and the ion screening parameter κa. (b) Free energies F for the three crystal structures (scaled by $F^* = a^3\sigma_+^2/\varepsilon\varepsilon_o$) with excess charge $\Delta\sigma/\sigma_+ = -0.1$; the solid black curve shows the free energy of two particles at infinite separation. For small κa, structures with more free volume are energetically favored ($F_{ZnS} < F_{NaCl} < F_{CsCl}$). For large κa, structures with more nearest neighbors are favored ($F_{CsCl} < F_{NaCl} < F_{ZnS}$). (c) Data from (b) presented as the energy of crystallization ΔF. Crystallization is energetically unfavorable for small κa due to excess charge.

weak screening ($\kappa a \ll 1$), the volume between the particles is filled with a nearly uniform concentration of free ionic charge to maintain the charge neutrality of the unit cell. The density of this ionic charge can be approximated as

$$\rho = \frac{4\pi a^2}{V_i}\Delta\sigma \tag{10}$$

where V_i is the interstitial volume (per ion pair) within the unit cell (here, V_i/a^3 = 3.94, 7.62, and 16.25 for CsCl, NaCl, and ZnS, respectively). The charge density is directly related to the potential through the Boltzmann equation

$$\rho = 2en_o \sinh\left(\frac{e\varphi}{k_BT}\right) \approx \varepsilon\varepsilon_o\kappa^2\varphi \tag{11}$$

where the approximation is consistent with the linear PB equation used here. Combining eqs 10 and 11, the potential inside of the unit cell is approximately uniform and equal to

$$\varphi \approx \frac{4\pi a^2\Delta\sigma}{\varepsilon\varepsilon_o\kappa^2 V_i} \tag{12}$$

Consequently, the free energy per pair of oppositely charged NPs F is well approximated as

$$F \approx \frac{4\pi a^2}{2}\varphi(\sigma_+ + \sigma_-) = \frac{8\pi^2F^*}{(V_i/a^3)(\kappa a)^2}\left(\frac{\Delta\sigma}{\sigma_+}\right)^2 \tag{13}$$

This limit is illustrated in Figure 3b by the solid curves. Interestingly, eq 13 suggests that structures with larger interstitial volumes have lower electrostatic free energies due to increased entropy of the neutralizing counterions; the ranking of lattice energies is then $\Delta F_{ZnS} < \Delta F_{NaCl} < \Delta F_{CsCl}$.

For sufficiently small screening parameters κa, the formation of any crystalline structure becomes energetically unfavorable. Using eq 13, the energy of crystallization is unfavorable for screening parameters

$$\kappa a \le \sqrt{\frac{2\pi}{(V_i/a^3)}}\left(\frac{\Delta\sigma}{\sigma_+}\right) \tag{14}$$

This approximate relation is valid for small amounts of excess charge (i.e., for $\Delta\sigma/\sigma_+ \ll 1$). For example, for $\Delta\sigma/\sigma_+ = 0.1$ as in Figure 3b, the CsCl lattice becomes energetically unfavorable for $\kappa a < 0.13$.

In the opposite limit of short screening lengths ($\kappa a \gg 1$), the free energy of crystallization remains dominated by nearest-neighbor interactions. Consequently, lattices with more nearest neighbors are energetically preferred, $\Delta F_{CsCl} < \Delta F_{NaCl} < \Delta F_{ZnS}$. In this limit, the free energy can be approximated by using analytical solutions for two oppositely charged spheres[25] (Supporting Information section 3); this is illustrated by the solid curves in Figure 3b for $\kappa a \gg 1$.

We have shown how slight asymmetries in the surface charge of oppositely charged colloidal particles can have a significant impact on the types of crystalline structures that form. In particular, when the screening length is larger than the size of the assembling particles ($\kappa a \ll 1$), charge asymmetry can lead to the formation of "open" structures, like the diamond-like ZnS structure. According to the model, the formation of the ZnS structure requires the condition that $\kappa a \approx |\Delta\sigma/\sigma_+| \ll 1$. For example, for particles with 1% charge asymmetry ($|\Delta\sigma/\sigma_+| = 0.01$), the screening length κ^{-1} must be ~100 times greater than the particle radius a. From a practical perspective, the maximum screening length in deionized water is on the order of ~1 μm. As the proposed mechanism requires that $\kappa a \ll 1$, the formation of diamond-like crystals through electrostatic interactions alone is likely limited to submicrometer colloids. Additional experiments investigating colloidal crystallization for different values of the excess charge $\Delta\sigma/\sigma_+$ and the screening parameter κa would be valuable in further validating the predictions of the model.

■ ASSOCIATED CONTENT

Supporting Information

(1) Effective dielectric constant of a core−shell particle; (2) effects of the particle dielectric constant; (3) analytical expressions for pairwise electrostatic interactions. This material is available free of charge via the Internet at http://pubs.acs.org.

dx.doi.org/10.1021/jz4006114 | J. Phys. Chem. Lett. 2013, 4, 1507−1511

AUTHOR INFORMATION

Corresponding Author

*E-mail: kjmbishop@engr.psu.edu (K.J.M.B.); grzybor@northwestern.edu (B.A.G.).

Notes

The authors declare no competing financial interest.

ACKNOWLEDGMENTS

This work was supported by the Nonequilibrium Energy Research Center, which is an Energy Frontier Research Center funded by the U.S. Department of Energy, Office of Science, Office of Basic Energy Sciences (Award No. DE-SC0000989).

REFERENCES

(1) van Blaaderen, A. Materials Science — Colloids Get Complex. *Nature* **2006**, *439*, 545−546.
(2) Galisteo-Lopez, J. F.; Ibisate, M.; Sapienza, R.; Froufe-Perez, L. S.; Blanco, A.; Lopez, C. Self-Assembled Photonic Structures. *Adv. Mater.* **2011**, *23*, 30−69.
(3) Hynninen, A. P.; Thijssen, J. H. J.; Vermolen, E. C. M.; Dijkstra, M.; Van Blaaderen, A. Self-Assembly Route for Photonic Crystals with a Bandgap in the Visible Region. *Nat. Mater.* **2007**, *6*, 202−205.
(4) Maldovan, M.; Thomas, E. L. Diamond-Structured Photonic Crystals. *Nat. Mater.* **2004**, *3*, 593−600.
(5) Meseguer, F. Colloidal Crystals as Photonic Crystals. *Colloid Surf., A* **2005**, *270*, 1−7.
(6) Ho, K. M.; Chan, C. T.; Soukoulis, C. M. Existence of a Photonic Gap in Periodic Dielectric Structures. *Phys. Rev. Lett.* **1990**, *65*, 3152−3155.
(7) Moroz, A. Metallo-Dielectric Diamond and Zinc-Blende Photonic Crystals. *Phys. Rev. B* **2002**, *66*, 115109.
(8) Garcia-Santamaria, F.; Miyazaki, H. T.; Urquia, A.; Ibisate, M.; Belmonte, M.; Shinya, N.; Meseguer, F.; Lopez, C. Nanorobotic Manipulation of Microspheres for On-Chip Diamond Architectures. *Adv. Mater.* **2002**, *14*, 1144−1147.
(9) Ngo, T. T.; Liddell, C. M.; Ghebrebrhan, M.; Joannopoulos, J. D. Tetrastack: Colloidal Diamond-Inspired Structure with Omnidirectional Photonic Band Gap for Low Refractive Index Contrast. *Appl. Phys. Lett.* **2006**, *88*, 241920.
(10) Sharp, D. N.; Turberfield, A. J.; Denning, R. G. Holographic Photonic Crystals with Diamond Symmetry. *Phys. Rev. B* **2003**, *68*, 205102.
(11) Sharma, V.; Xia, D. Y.; Wong, C. C.; Carter, W. C.; Chiang, Y. M. Templated Self-Assembly of Non-Close-Packed Colloidal Crystals: Toward Diamond Cubic and Novel Heterostructures. *J. Mater. Res.* **2011**, *26*, 247−253.
(12) Bartlett, P.; Campbell, A. I. Three-Dimensional Binary Superlattices of Oppositely Charged Colloids. *Phys. Rev. Lett.* **2005**, *95*, 128302.
(13) Shevchenko, E. V.; Talapin, D. V.; Kotov, N. A.; O'Brien, S.; Murray, C. B. Structural Diversity in Binary Nanoparticle Superlattices. *Nature* **2006**, *439*, 55−59.
(14) Leunissen, M. E.; Christova, C. G.; Hynninen, A. P.; Royall, C. P.; Campbell, A. I.; Imhof, A.; Dijkstra, M.; van Roij, R.; van Blaaderen, A. Ionic Colloidal Crystals of Oppositely Charged Particles. *Nature* **2005**, *437*, 235−240.
(15) Kalsin, A. M.; Fialkowski, M.; Paszewski, M.; Smoukov, S. K.; Bishop, K. J. M.; Grzybowski, B. A. Electrostatic Self-Assembly of Binary Nanoparticle Crystals with a Diamond-Like Lattice. *Science* **2006**, *312*, 420−424.
(16) Kalsin, A. M.; Grzybowski, B. A. Controlling the Growth of "Ionic" Nanoparticle Supracrystals. *Nano Lett.* **2007**, *7*, 1018−1021.
(17) Rechtsman, M. C.; Stillinger, F. H.; Torquato, S. Synthetic Diamond and Wurtzite Structures Self-Assemble with Isotropic Pair Interactions. *Phys. Rev. E* **2007**, *75*, 031403.
(18) Zhang, Z. L.; Keys, A. S.; Chen, T.; Glotzer, S. C. Self-Assembly of Patchy Particles into Diamond Structures through Molecular Mimicry. *Langmuir* **2005**, *21*, 11547−11551.
(19) Witt, D.; Klajn, R.; Barski, P.; Grzybowski, B. A. Applications Properties and Synthesis of Omega-Functionalized N-Alkanethiols and Disulfides — The Building Blocks of Self-Assembled Monolayers. *Curr. Org. Chem.* **2004**, *8*, 1763−1797.
(20) Leff, D. V.; Ohara, P. C.; Heath, J. R.; Gelbart, W. M. Thermodynamic Control of Gold Nanocrystal Size — Experiment and Theory. *J. Phys. Chem.* **1995**, *99*, 7036−7041.
(21) Sellers, H.; Ulman, A.; Shnidman, Y.; Eilers, J. E. Stucture and Binding of Alkanethiolates on Gold and Silver Surfaces — Implications for Self-Assembled Monolayers. *J. Am. Chem. Soc.* **1993**, *115*, 9389−9401.
(22) Russel, W. B.; Saville, D. A.; Schowalter, W. R. *Colloidal Dispersions*; Cambridge University Press: New York; 1989.
(23) Verwey, E. J. W.; Overbeek, J. T. G. *Theory of the Stability of Lyophobic Colloids*; Elsevier: New York; 1948.
(24) Kittel, C. *Introduction to Solid State Physics*; John Wiley & Sons: New York; 2005.
(25) Carnie, S. L.; Chan, D. Y. C.; Gunning, J. S. Electrical Double-Layer Interaction between Dissimilar Spherical Colloidal Particles and between a Sphere and a Plate — The Linearized Poisson−Boltzmann Theory. *Langmuir* **1994**, *10*, 2993−3009.